ADVANCES IN ATMOSPHERIC SCIENCES, VOL. 34, NOVEMBER 2017, 1282–1289

• **Original Paper** •

Decadal Indian Ocean Dipolar Variability and Its Relationship with the Tropical Pacific

Yun YANG*[1], Jianping LI[1,2], Lixin WU[3], Yu KOSAKA[4], Yan DU[5], Cheng SUN[1], Fei XIE[1], and Juan FENG[1]

[1]*State Key Laboratory of Earth Surface Processes and Resource Ecology and College of Global Change and Earth System Science, Beijing Normal University, Beijing* 100875*, China*

[2]*Laboratory for Regional Oceanography and Numerical Modeling, Qingdao National Laboratory for Marine Science and Technology, Qingdao* 266237*, China*

[3]*Physical Oceanography Laboratory/Qingdao Collaborative Innovation Center of Marine Science and Technology, Ocean University of China, Qingdao* 266003*, China*

[4]*Research Center for Advanced Science and Technology, University of Tokyo, Tokyo* 153-8904*, Japan*

[5]*State Key Laboratory of Tropical Oceanography, South China Sea Institute of Oceanology, Chinese Academy of Sciences, Guangzhou* 510301*, China*

(Received 12 January 2017; revised 3 April 2017; accepted 15 May 2017)

ABSTRACT

A robust decadal Indian Ocean dipolar variability (DIOD) is identified in observations and found to be related to tropical Pacific decadal variability (TPDV). A Pacific Ocean–global atmosphere (POGA) experiment, with fixed radiative forcing, is conducted to evaluate the DIOD variability and its relationship with the TPDV. In this experiment, the sea surface temperature anomalies are restored to observations over the tropical Pacific, but left as interactive with the atmosphere elsewhere. The TPDV-forced DIOD, represented as the ensemble mean of 10 simulations in POGA, accounts for one third of the total variance. The forced DIOD is triggered by anomalous Walker circulation in response to the TPDV and develops following Bjerknes feedback. Thermocline anomalies do not exhibit a propagating signal, indicating an absence of oceanic planetary wave adjustment in the subtropical Indian Ocean. The DIOD–TPDV correlation differs among the 10 simulations, with a low correlation corresponding to a strong internal DIOD independent of the TPDV. The variance of this internal DIOD depends on the background state in the Indian Ocean, modulated by the thermocline depth off Sumatra/Java.

Key words: Indian Ocean dipole, decadal variability, tropical Pacific decadal variability

Citation: Yang, Y., J. P. Li, L. X. Wu, Y. Kosaka, Y. Du, C. Sun, F. Xie, and J. Feng, 2017: Decadal Indian Ocean dipolar variability and its relationship with the tropical Pacific. *Adv. Atmos. Sci.*, **34**(11), 1282–1289, https://doi.org/10.1007/s00376-017-7009-2.

1. Introduction

The Indian Ocean dipole (IOD), featuring an east–west zonal sea surface temperature (SST) dipole, is the leading interannual variability over the tropical Indian Ocean (Saji et al., 1999; Webster et al., 1999). The IOD has been studied extensively due to its significant impact on the Asian monsoon (Guan et al., 2003; Saji and Yamagata, 2003; Yamagata et al., 2004) and El Niño–Southern Oscillation (ENSO; Yu et al., 2002; Kug and Kang, 2006; Luo et al., 2010).

In addition to interannual variations, the IOD index exhibits variability on decadal and longer timescales [see the review by Han et al. (2014b)]. Analyzing coral records, Abram et al. (2008) reported an increase in the frequency and amplitude of IOD events in the 20th century. Observations and modeling studies reveal an increasing trend of IOD index and skewness under global warming (Ihara et al., 2008; Cai et al., 2009, 2014) and, overlying this trend, are decadal oscillations. Based on observational data, Ashok et al. (2004) demonstrated IOD-like 8–25-yr decadal fluctuations. Such decadal Indian Ocean dipolar variability (DIOD) has also been noted in modeling studies (Tozuka et al., 2007; Zheng et al., 2010).

The phenomenon of DIOD has received little attention and its dynamics remain elusive. Ashok et al. (2004) suggested the importance of oceanic dynamics, due to the high correlation between the DIOD and thermocline depth anomalies over the Indian Ocean. However, the cross-basin timescale of low-latitude Rossby waves is too short to sus-

* Corresponding author: Yun YANG
Email: yunyang@bnu.edu.cn

tain decadal variability. Tozuka et al. (2007) interpreted the DIOD as the residual of skewness (asymmetry of positive and negative events) of the interannual IOD.

Influence from the tropical Pacific is controversial. ENSO is an important trigger of the IOD (e.g., Yu and Lau, 2004; Yang et al., 2015), while previous studies suggest little influence of the DIOD from the tropical Pacific decadal variability (TPDV) (Ashok et al., 2004; Tozuka et al., 2007). Using GISST data, Ashok et al. (2004) noted a low correlation between the DIOD and TPDV during 1950–99, and a similar finding was reported from modeling results (Tozuka et al., 2007). However, the TPDV exerts significant influence on the Walker circulation, Indonesian throughflow, and the climatology of the Indian Ocean (Allan et al., 1995; Lee and McPhaden, 2008; Zheng et al., 2010). Such influences can affect the DIOD, and thus the low DIOD–TPDV correlation requires further study.

In this paper, we find that the DIOD is robust in observations and that the TPDV significantly influences the DIOD via changing the Walker circulation. Their correlation, as modulated by the DIOD's internal activity, is associated with the thermocline depth off Sumatra/Java. Following this introduction, section 2 introduces the data and methods used in the study. Section 3 analyzes the DIOD in observations. Section 4 studies the influence of the TPDV on the DIOD. The paper concludes with a summary and discussion in section 5.

2. Data and methods

In this study, we use observational monthly SST data from the Hadley Centre Sea Ice and Sea Surface Temperature dataset (HadISST; Rayner et al., 2003), version 2 of the Kaplan Extended SST dataset (Kaplanv2; Kaplan et al., 1998), and version 2 of the Centennial Observation-Based Estimates of SST dataset (COBE-SST2; Hirahara et al., 2014), during the period 1870–2012. All data are detrended and 8-yr low (high)-pass filtered to represent the decadal (interannual) variability.

In addition, we use Pacific Ocean–global atmosphere (POGA) experiment, based on version 2.1 of the Geophysical Fluid Dynamics Laboratory's Climate Model (Delworth et al., 2006). The SST over the central–eastern (15°S–15°N, 180°E–coast) tropical Pacific is restored to the observed (HadISST) anomalies plus model climatology (preindustrial run), but left interactive with the atmosphere elsewhere. POGA is conducted to eliminate the distortion caused by model-biased tropical Pacific variability. It consists of 10 simulations with slightly different initial conditions in the year 1940, and we use the period 1950–2012. The details of this experiment are documented in Kosaka and Xie (2013). The radiative forcing of the POGA experiment in this paper, however, is fixed at the level in 1990, instead of following the historical variations in Kosaka and Xie (2013), in order to suppress the influence of global warming. The observed Indian Ocean experiences rapid warming after 1950s, with a trend of 0.11°C (10 yr)$^{-1}$ (Fig. 1). In POGA, however, the trend is significantly reduced, at 0.02°C (10 yr)$^{-1}$.

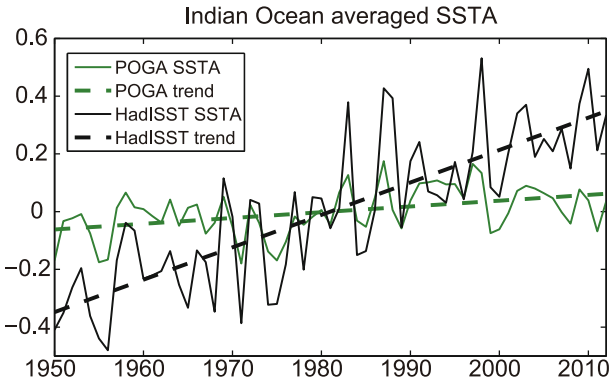

Fig. 1. Time series (°C) and the trend of the Indian Ocean–averaged annual mean SST anomaly (SSTA) (20°S–30°N, 40°–120°E), using the POGA ensemble mean and HadISST data, during 1950–2012.

POGA is helpful for extracting the tropical Pacific forced variability. We use the ensemble mean and residual of the 10 simulations to represent the tropical Pacific forced and internal variability in POGA (also see Kosaka et al., 2013; Yang et al., 2015, 2017).

On the decadal timescale, the first empirical orthogonal function (EOF) mode of the tropical Pacific (20°S–20°N, 120°E–60°W), explaining 53% of total variance, resembles the spatial pattern of the Interdecadal Pacific Oscillation [IPO; EOF1 over the entire Pacific (40°S–60°N, 120°E–60°W)]. The spatial pattern of these two EOF modes is ENSO-like. The correlation coefficient of the two PC1s (first principal components) reaches 0.96, indicating a tight relationship between the IPO and TPDV. Moreover, the two PC1s are highly correlated with the 8-yr low-pass filtered Niño3.4 index [SST averaged over (5°S–5°N, 120°–170°W)], with correlation coefficients of 0.95 and 0.94, respectively. The result is consistent with previous findings (e.g., Power et al., 1999; Meehl and Hu, 2006). The above analysis is based on HadISST and is consistent with that in Kaplanv2, COBE-SST2 and POGA. Hereafter, we use this low-pass filtered Niño3.4 index to represent the TPDV index.

3. DIOD in observations

At the interannual timescale, the IOD emerges as the second EOF mode of the boreal autumn SST anomalies over the tropical Indian Ocean (20°S–20°N, 40°–120°E) during 1870–2012 (Fig. 2a). The spatial pattern of EOF2 resembles the IOD, but with the western pole centered in the Southern Hemisphere. This difference might be due to the different period of data used in the studies. In response to the IOD, the SST anomalies display an El Niño-like pattern over the Pacific Ocean (Fig. 2b). The correlation between PC2 and the 8-yr high-pass filtered Niño3.4 index in boreal autumn is 0.28 (significant at the 95% confidence level). This result is consistent with previous findings that the IOD can be triggered by both ENSO forcing and ocean–atmosphere feedbacks internal to the Indian Ocean (Luo et al., 2010; Yang et al., 2015).

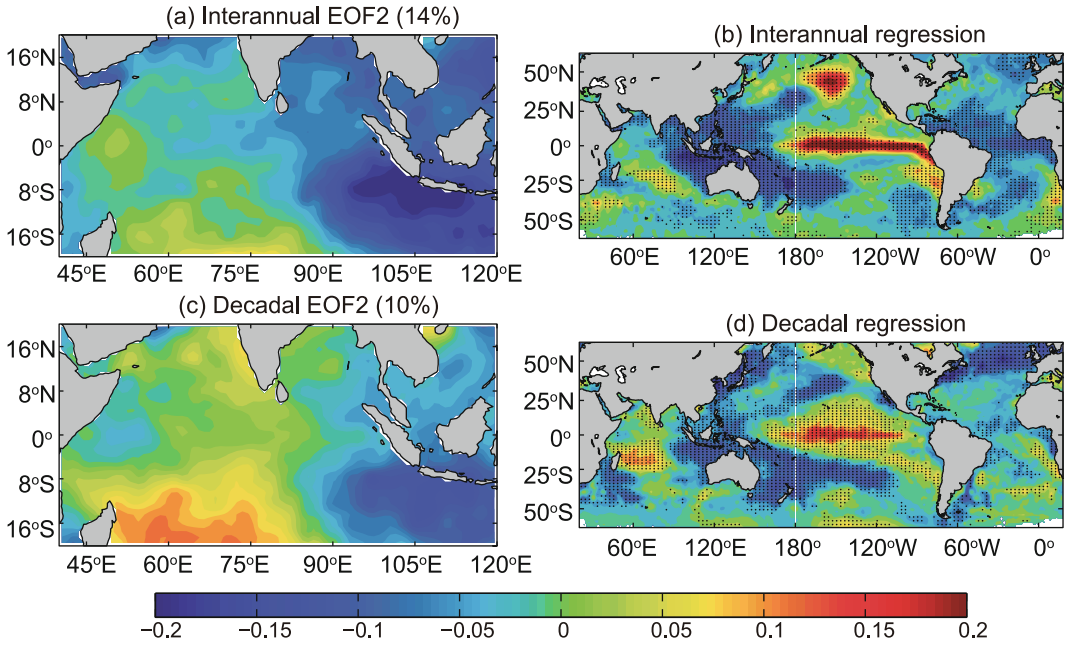

Fig. 2. The second EOF modes of (a, b) interannual and (c, d) decadal SST variability over the Indian Ocean (20°S–20°N, 40°–120°E) in August–September–October (ASO) during 1870–2012, based on HadISST: (a, c) the EOF patterns and (b, d) regressed ASO SST anomalies against the corresponding PCs. The dotted areas are statistically significant at the 5% level. Units: °C.

At the decadal timescale, EOF2, explaining 10% of the total variance, features a robust variability (Fig. 2c). The spatial pattern of this mode resembles that of the interannual IOD (spatially correlated at 0.89), except for a relatively stronger western pole. We call this zonal dipole-like mode the DIOD. As in the interannual IOD, the DIOD also features its strongest variability in boreal autumn (not shown). In addition, the EOF1 of the decadal SST anomalies displays basin-wide warming/cooling (not shown), and we call this the decadal Indian Ocean basin mode (DIOB).

The DIOD is closely associated with variations over the tropical Pacific. The Pacific exhibits an IPO-like pattern in association with the DIOD (Fig. 2d). Compared to ENSO, the IPO exhibits a wider meridional spatial pattern, in concert with the involvement of higher latitude oceanic Rossby waves (e.g., Chen and Wallace, 2015). The correlation between PC2 and the 8-yr low-pass filtered Niño3.4 index in boreal autumn is 0.49 (significant at the 95% confidence level).

The robust DIOD variability and its significant association with the IPO can also be observed in the Kaplanv2 and COBE-SST2 datasets (Fig. 3). In these two datasets, the DIOD emerges as the second EOF mode, explaining 13% and 10% of the total variance, respectively. The correlation coefficients between the DIOD and the low-pass filtered Niño3.4 index reach 0.50 and 0.47 (significant at the 95% confidence level)—similar to HadISST.

4. Tropical Pacific influence on the DIOD

The POGA experiment is conducted to study the dynamics of the DIOD and its relationship with the tropical Pacific. The effect of global warming is eliminated by fixing the radiative forcing.

POGA has good simulation skill with respect to the observed Indian Ocean SST variability, including the mean state and the IOD (Yang et al., 2015). In POGA, the DIOD displays a zonal SST gradient pattern and peaks in boreal autumn (September–October–November; SON). However, it emerges as the leading EOF mode and shows a stronger variance than observed (not shown). Such a bias might be due to a shallower mixed-layer depth off Sumatra/Java. Moreover, the SST features stronger anomalies over the northwestern tropical Indian than observed. Such a spatial pattern in POGA resembles the interannual IOD in previous studies (Saji et al., 1999). The PC1 is tightly correlated with the dipole mode index [DMI, defined as the SST difference between (10°S–10°N, 50°–70°E) and (10°S–0°, 90°–110°E)], with a correlation coefficient reaching 0.97. Here, we use the 8-yr low-pass filtered DMI to represent the DIOD variations in the POGA experiment.

The ensemble mean of the decadal DMI co-varies with the TPDV index, with a maximum correlation of 0.85 at lag = 0 (Fig. 4). This indicates that the ensemble mean of POGA is an effective way to extract the TPDV-forced DIOD. The forced variability, accounting for 38% of the DMI decadal variance (calculated as the ratio of decadal DMI variance between the ensemble mean and raw data), is an important component of the DIOD.

The forced DIOD develops following Bjerknes feedback (Bjerknes, 1969), as in the interannual IOD. Two years before the DIOD peaks (lag = −2 yr), the wind anomalies turn into easterlies along the equator (Fig. 5b2). Such wind anomalies

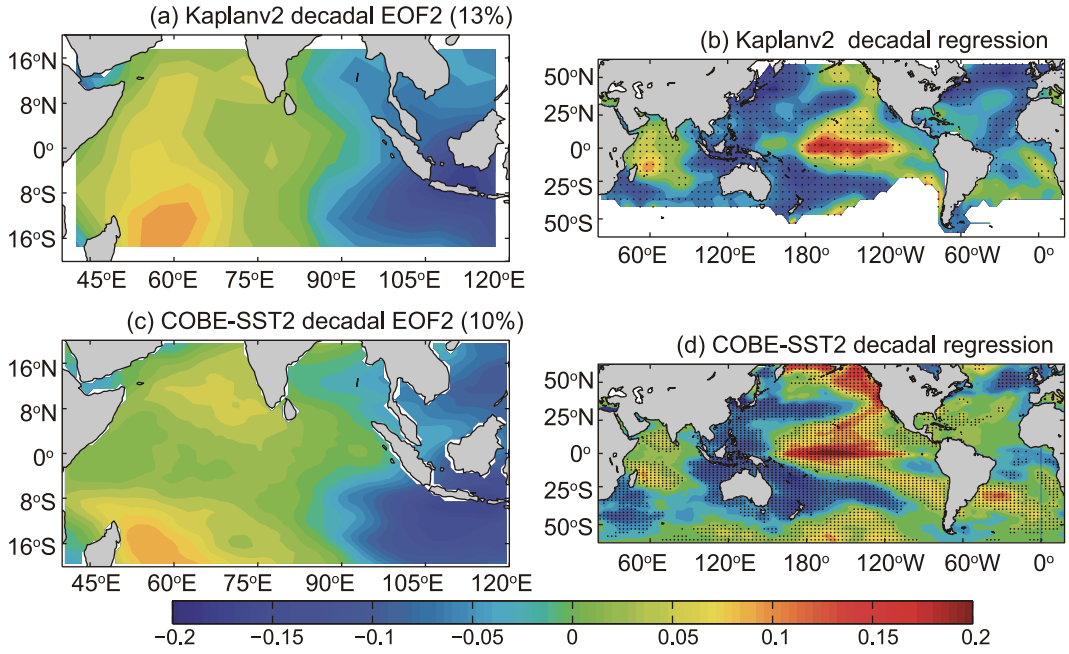

Fig. 3. As in Fig. 2, but for decadal variability using the (a, b) Kaplanv2 and (c, d) COBE-SST2 datasets.

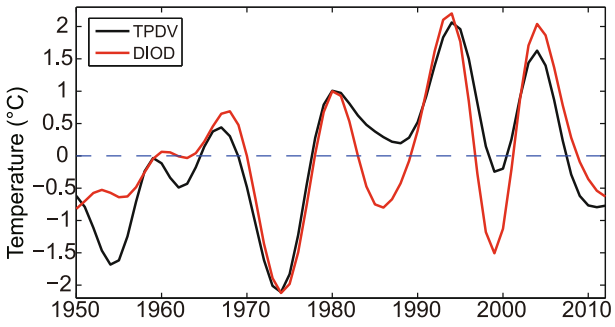

Fig. 4. The DIOD [PC1 of the 8-yr low-pass filtered SON SST over the Indian Ocean (20°S–20°N, 40°–120°E)] and the standardized TPDV indices in SON, based on the POGA ensemble mean.

shoal (deepen) the thermocline depth and lead to the SST cooling (warming) over the eastern (western) equatorial Indian Ocean (Figs. 5b1 and 5b2). The DIOD grows following this positive Bjerknes feedback, consistent with the interannual IOD (Yang et al., 2015). The strong equatorial easterly anomalies form a pair of anticyclonic wind stress curls straddling the equator, which deepens the thermocline and warms the SST. This thermocline effect, however, is offset by heat flux anomalies over the southwestern Indian Ocean. The heat flux acts to decrease the SST anomalies over the eastern Indian Ocean, in contrast to Tozuka et al. (2007). This damping effect of heat flux might be related to strong Newtonian cooling in response to the overestimated SST anomalies (Xie et al., 2010; Yang et al., 2015).

The evolution of the DIOD is sustained by the equatorial wind anomalies. The equatorial easterly anomalies first appear off the coast of Sumatra/Java, corresponding to the local development of SST anomalies. They then strengthen (weaken) during the developing (decaying) period (Figs. 5b–d) and turn into westerlies at lag = 4 yr, in concert with the phase transition of the DIOD (Fig. 5e).

The cross-basin Rossby wave in the midlatitudes is found to be unrelated to the evolution of forced DIOD variability. Previous studies have proposed that the decadal "memory" of the Pacific Decadal Oscillation and North Atlantic Tripole can be achieved via midlatitude oceanic Rossby waves (Wu et al., 2003, Yang et al., 2012). This dynamic, however, is not responsible for the evolution of the DIOD. The regressed $Z20$ (20°C isothermal depth) exhibits no propagation signal on the decadal timescale over the subtropical Indian basin (not shown).

The wind anomalies over the equatorial Indian Ocean are triggered by the TPDV via the anomalous Walker circulation (Fig. 6). The regressed anomalies exhibit a typical positive IPO phase (Figs. 2d and 6e). Over the Pacific, the SST anomalies display widescale warming over the tropics and cooling over the western subtropics. The corresponding sea level pressure (SLP) anomalies display a canonical Southern Oscillation and enhanced Aleutian Low pattern, consistent with previous studies (Fig. 6; Zhang et al., 1997; Chen and Wallace, 2015). The center of the simulated TPDV, however, is shifted westwards compared to observations, due to model bias. The TPDV weakens the Walker circulation, forces anomalous equatorial surface easterlies over the Indian Ocean, and triggers the DIOD. The development of the DIOD closely follows that of the TPDV and shifts its phase at the emergence of negative IPO (Fig. 6i).

The DIOD–TPDV correlation varies among the 10 simulations of POGA. The correlation coefficients range from 0.15 to 0.77, with an average of 0.45. We select the runs

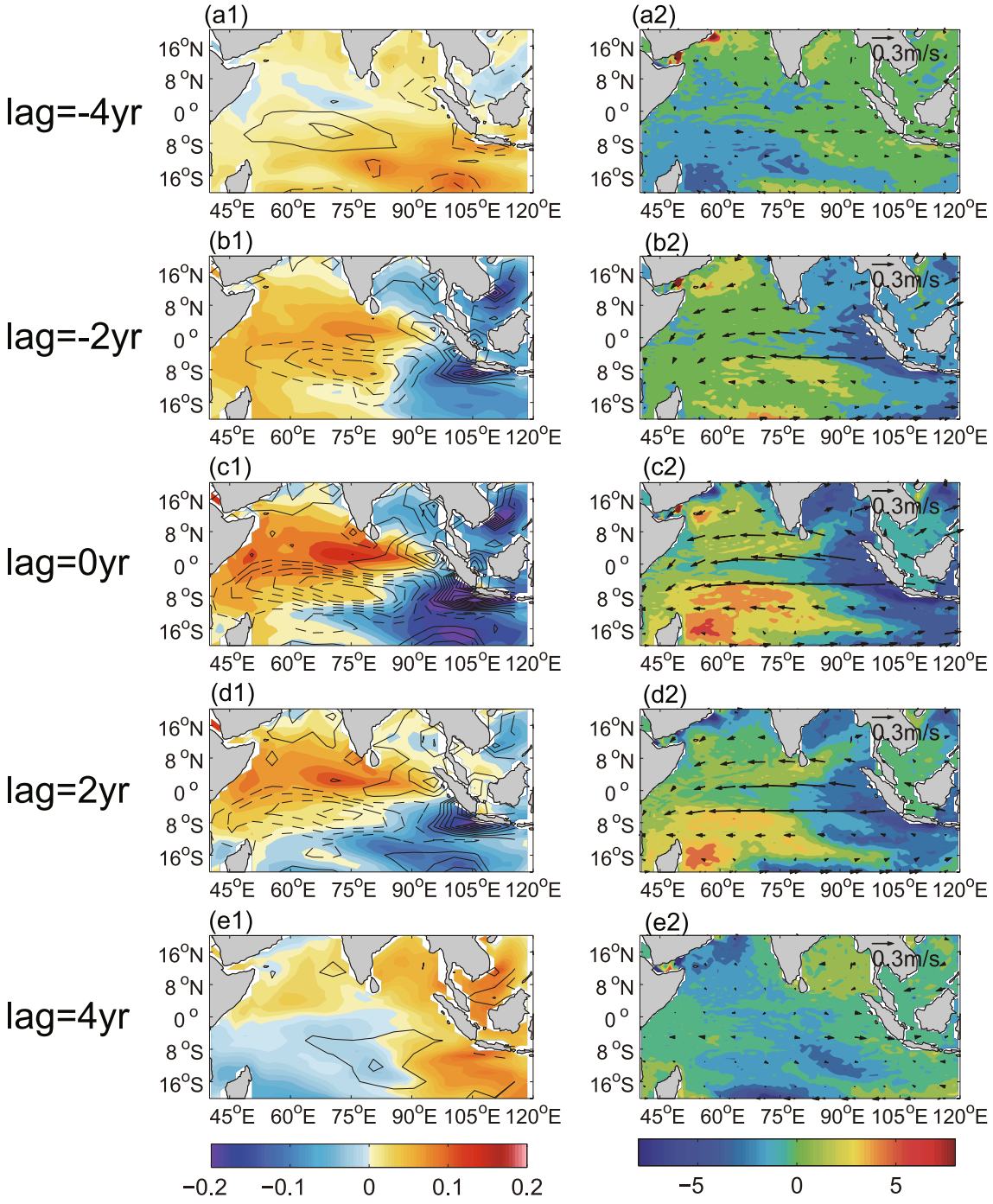

Fig. 5. Lagged regression of (left) SST (°C; color shading) and surface heat flux (W m^{-2}; contours; solid to heat the ocean), and (right) *Z*20 (m; color shading) and surface wind velocity (m s^{-1}; vectors), against the DIOD, shown for lags of every other year as indicated. All data are based on the POGA experiment and are 8-yr low-pass filtered to retain decadal variability.

with minimum (run_3) and maximum (run_7) correlation coefficients and study their differences. The DIOD in a single member is composed of the TPDV-forced and internal variability. A strong variance of either component would compromise the correlation between the other component and the DIOD. As a result, the variance of the internal DIOD in run_3 (0.1176°C^2) is about 2.5 times larger than that of run_7 (0.0477°C^2). Such a difference originates in the mean state (Fig. 7). The climatological difference (run_3 minus run_7) displays a positive IOD-like pattern, with easterlies and a westward SST gradient along the equator. The shoaling of the thermocline off Sumatra/Java would intensify the thermocline feedback, enhance the DIOD internal variability, and weaken the correlation between the DIOD and TPDV. This has also been suggested for the interannual IOD (Saji et al., 2006; Zheng et al., 2010; Yang et al., 2015). The climato-

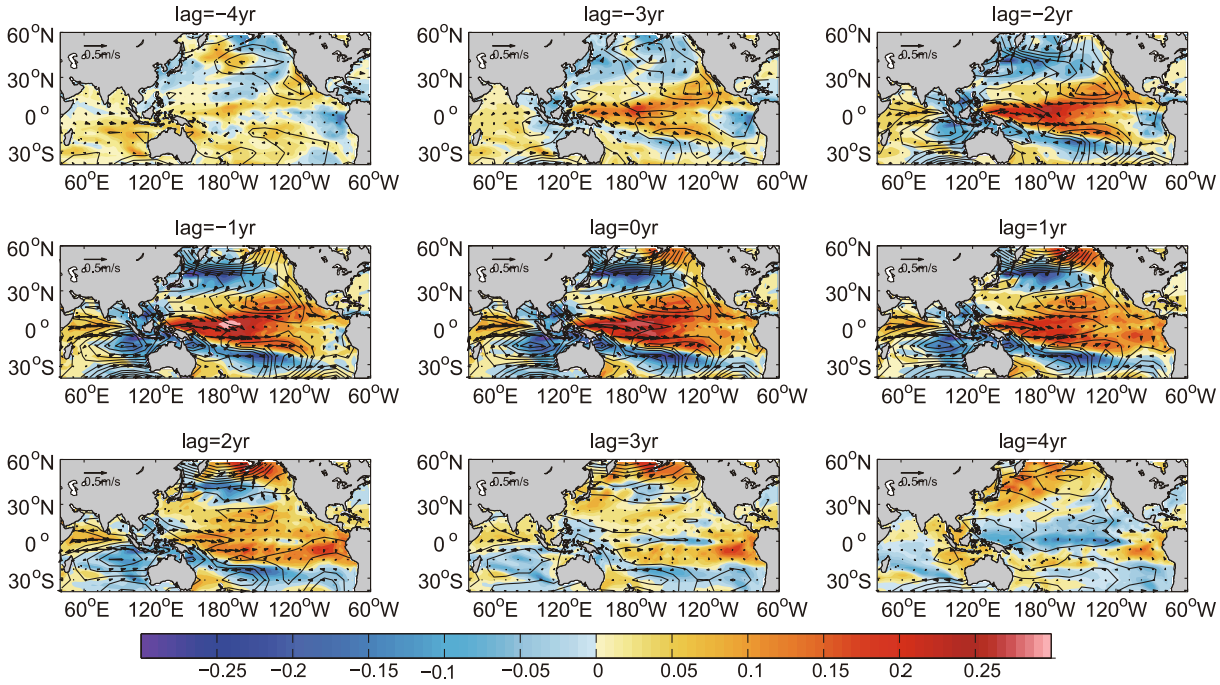

Fig. 6. As in Fig. 5, but for SST (°C; color shading), SLP (hPa; contours at 0.05 intervals) and surface wind velocity (m s^{-1}; vectors) anomalies, shown for lags of every year as indicated.

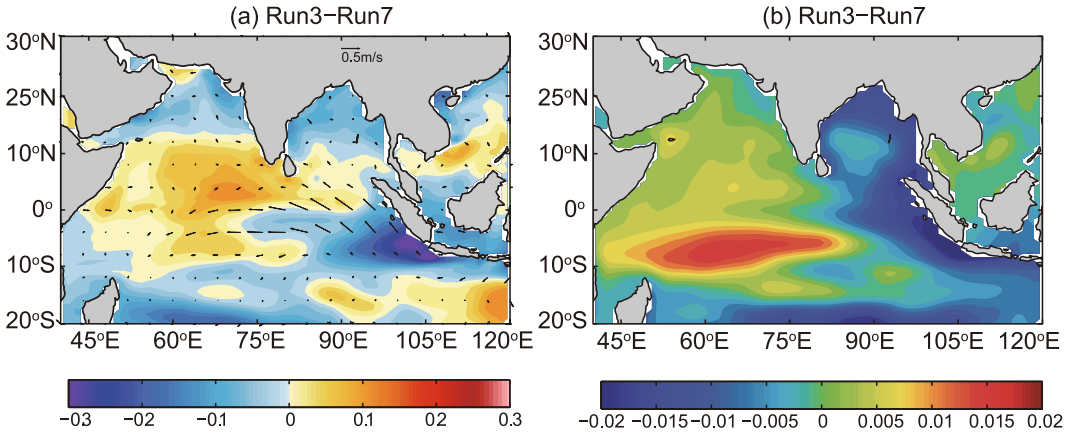

Fig. 7. Climatological difference of SON (a) SST (°C; color shading) and surface wind velocity (m s^{-1}; vectors) and (b) sea surface height (m) between the 3rd and 7th members of POGA.

logical difference might be due to multidecadal or centennial IOD-like variability.

5. Summary and discussion

The observed IOD displays robust decadal oscillations that are related to the TPDV. An experiment (POGA) is conducted to study the influence of the TPDV on the DIOD. In this experiment, the SST anomalies are restored to observations over the tropical Pacific, while fully coupled to the atmosphere over the rest of the world's oceans. The radiative forcing is fixed at the level in 1990 to eliminate the effect of global warming. POGA consists of 10 simulations, during the period 1950–2012. The ensemble mean represents the TPDV-forced variability, accounting for about one third of the total variance. The TPDV-forced DIOD is triggered by anomalous Walker circulation and develops through Bjerknes feedback. The thermocline depth anomalies, however, exhibit no signal of propagation, indicating an absence of oceanic planetary wave adjustment in the subtropical Indian Ocean. The DIOD–TPDV correlation, associated with the climatology over the Indian Ocean, varies among the 10 simulations. The shoaling of the thermocline off Sumatra/Java enhances the thermocline feedback, strengthens the DIOD internal variability, and diminishes the DIOD–TPDV correlation.

It is important to note that the result of the DIOD variability relies on the definition of the index. In Fig. 2, the

SST anomalies of the western pole are larger in the Southern Hemisphere (especially south of 10°S) than in the Northern Hemisphere at decadal timescale. Previous studies (e.g., Saji et al., 1999), however, suggest prominent SST anomalies over tropical western basin (10°S-10°N) at interannual timescale. This spatial difference might be related to the different periods of data used in studies. Therefore, using HadISST over 1870–2012, the DMI index might not properly depict the zonal SST gradient of the DIOD. Moreover, the DMI after the 1950s is notably contaminated by the global warming signal. During this period, the Indian Ocean experiences sustained warming, with a larger ratio over the western tropical Indian than over the eastern basin. The DMI index, defined as the east–west SST gradient, is notably contaminated by this spatially non-uniform warming trend (Fig. 8). The DMI shows intensified variability during 1950–70. Thereafter, it displays a rapid increasing trend and weakened decadal oscillations. The correlation coefficients between PC2 and the DMI before and after the 1950s are 0.65 and 0.16 (after detrending), respectively. In POGA, however, the DMI describes the spatial pattern of the DIOD very well, probably due to the suppressed effect of global warming in response to the fixed radiative forcing (Fig. 5). The correlation between PC1 and the DMI reaches 0.97.

One interesting issue concerning the DIOD–TPDV relationship is that our result contradicts previous findings. Ashok et al. (2004) suggested a low DMI–Niño3 correlation on the decadal timescale during the period 1950–99. This contradiction might be due to two factors. First, the definition of the DIOD plays an important role. The DMI index might not be adequate in representing the DIOD variability, especially after the 1950s. Second, the decadal DMI-Niño3 relationship might be weakened by the effect of global warming during this period. The Indian Ocean features suppressed equatorial westerly winds and shoaling of the thermocline off Sumatra/Java in response to global warming—a result shown in both observations and climate models (e.g., Cai et al., 2014; Dong et al., 2014). Such changes would weaken the decadal DMI–Niño3 correlation by enhancing the thermocline feedback and strengthening the DIOD internal variability, as discussed in section 4. Although the DIOD is associated with the TPDV during 1950–2012, this variability does not display an IPO-like spatial pattern (not shown).

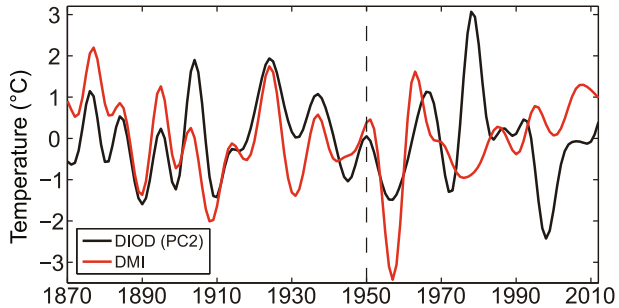

Fig. 8. Observed time series of the DIOD (PC2) and decadal (8-yr low pass-filtered) DMI (°C), during the period 1870–2012.

Some other changes of Indo-Pacific decadal covariability have been suggested in previous studies. The relationship between the DIOB and IPO changes from being in-phase before 1985 to out-of-phase thereafter (Han et al., 2014a). The stronger (relative to the Pacific's) warming rate of the Indian Ocean might be responsible for the recent phase transition of the IPO and the global warming hiatus, via strengthening the Walker circulation (Luo et al., 2012; Han et al., 2014a; Dong et al., 2016). This indicates the Indo-Pacific inter-basin coupling might have undergone significant changes in recent decades, due to the sustained robust warming over the Indian Ocean.

Acknowledgements. This work is supported by National Key R&D Program of China (2016YFA0601803), National Natural Science Foundation of China (NSFC) project (41606008, 41525019), the State Oceanic Administration of China (GASI-IPOVAI-02), the State Key Laboratory of Tropical Oceanography, South China Sea Institute of Oceanology, Chinese Academy of Sciences (Project No. LTO1603), the Japan Society for the Promotion of Science [Grant-in-Aid for Young Scientists (A) JP15H05466], and the Japanese Ministry of Environment (Environment Research and Technology Development Fund 2-1503).

REFERENCES

Abram, N. J., M. K. Gagan, J. E. Cole, W. S. Hantoro, and M. Mudelsee, 2008: Recent intensification of tropical climate variability in the Indian Ocean. *Nat. Geosci*., **1**, 849–853, doi: 10.1038/ngeo357.

Allan, R. J., J. A. Lindesay, and C. J. C. Reason, 1995: Multidecadal variability in the climate system over the Indian Ocean region during the austral summer. *J. Climate*, **8**, 1853–1873, doi: 10.1175/1520-0442(1995)008<1853:MVITCS>2.0.CO;2.

Ashok, K., W.-L. Chan, T. Motoi, and T. Yamagata, 2004: Decadal variability of the Indian Ocean dipole. *Geophys. Res. Lett*., **31**, L24207, doi: 10.1029/2004GL021345.

Bjerknes, J., 1969: Atmospheric teleconnections from the equatorial Pacific. *Mon. Wea. Rev*., **97**, 163–172, doi: 10.1175/1520-0493(1969)097<0163:ATFTEP>2.3.CO;2.

Cai, W., T. Cowan, and A. Sullivan, 2009: Recent unprecedented skewness towards positive Indian Ocean dipole occurrences and its impact on Australian rainfall. *Geophys. Res. Lett*., **36**, L11705, doi: 10.1029/2009GL037604.

Cai, W. J., A. Santoso, G. J. Wang, E. Weller, L. X. Wu, K. Ashok, Y. Masumoto, and T. Yamagata, 2014: Increased frequency of extreme Indian Ocean Dipole events due to greenhouse warming. *Nature*, **510**, 254–258, doi: 10.1038/nature13327.

Chen, X. Y., and J. M. Wallace, 2015: ENSO-like variability: 1900–2013. *J. Climate*, **28**, 9623–9641, doi: 10.1175/JCLI-D-15-0322.1.

Delworth, T. L., and Coauthors, 2006: GFDL's CM2 global coupled climate models. Part I: Formulation and simulation characteristics. *J Climate*, **19**, 643–674, doi: 10.1175/JCLI3629.1.

Dong, L., T. J. Zhou, and B. Wu, 2014: Indian Ocean warming during 1958-2004 simulated by a climate system model and its mechanism. *Climate Dyn*., **42**, 203–217, doi: 10.1007/s00382-013-1722-z.

Dong, L., T. J. Zhou, A. G. Dai, F. F. Song, B. Wu, and X. L. Chen,

2016: The footprint of the inter-decadal Pacific oscillation in Indian Ocean sea surface temperatures. *Sci. Rep*., **6**, 21251, doi: 10.1038/srep21251.

Guan, Z. Y., K. Ashok, and T. Yamagata, 2003: Summertime response of the tropical atmosphere to the Indian Ocean dipole sea surface temperature anomalies. *J. Meteor. Soc. Japan*, **81**, 531–561, doi: 10.2151/jmsj.81.533.

Han, W. Q., and Coauthors, 2014a: Intensification of decadal and multi-decadal sea level variability in the western tropical Pacific during recent decades. *Climate Dyn*., **43**, 1357–1379, doi: 10.1007/s00382-013-1951-1.

Han, W. Q., J. Vialard, M. J. McPhaden, T. Lee, Y. Masumoto, M. Feng, and W. P. M. de Ruijter, 2014b: Indian Ocean decadal variability: A review. *Bull. Amer. Meteor. Soc*., **95**, 1679–1703, doi: 10.1175/BAMS-D-13-00028.1.

Hirahara, S., M. Ishii, and Y. Fukuda, 2014: Centennial-scale sea surface temperature analysis and its uncertainty. *J. Climate*, **27**, 57–75. doi: 10.1175/JCLI-D-12-00837.1.

Ihara, C., Y. Kushnir, and M. A. Cane, 2008: Warming trend of the Indian Ocean SST and Indian Ocean dipole from 1880 to 2004. *J. Climate*, **21**, 2035–2046, doi: 10.1175/2007JCLI1945.1.

Kaplan, A., M. A. Cane, Y. Kushnir, A. C. Clement, M. B. Blumenthal, and B. Rajagopalan, 1998: Analyses of global sea surface temperature 1856–1991. *J. Geophys. Res*., **103**(C9), 18 567–18 589, doi: 10.1029/97JC01736.

Kosaka, Y., and S.-P. Xie, 2013: Recent global-warming hiatus tied to equatorial Pacific surface cooling. *Nature*, **501**, 403–407, doi: 10.1038/nature12534.

Kosaka, Y., S.-P. Xie, N.-C. Lau, and G. A. Vecchi, 2013: Origin of seasonal predictability for summer climate over the Northwestern Pacific. *Proceedings of the National Academy of Sciences of the United States of America*, **110**, 7574–7579, doi: 10.1073/pnas.1215582110.

Kug, J.-S., and I.-S. Kang, 2006: Interactive feedback between ENSO and the Indian Ocean. *J Climate*, **19**, 1784–1801, doi: 10.1175/JCLI3660.1.

Lee, T., and M. J. McPhaden, 2008: Decadal phase change in large-scale sea level and winds in the Indo-Pacific region at the end of the 20th century. *Geophys. Res. Lett*., **35**, L01605, doi: 10.1029/2007GL032419.

Luo, J. J., R. C. Zhang, S. K. Behera, Y. Masumoto, F.-F. Jin, R. Lukas, and T. Yamagata, 2010: Interaction between El Niño and extreme Indian Ocean dipole. *J. Climate*, **23**, 726–742, doi: 10.1175/2009JCLI3104.1.

Luo, J. J., W. Sasaki, and Y. Masumoto, 2012: Indian Ocean warming modulates Pacific climate change. *Proceedings of the National Academy of Sciences of the United States of America*, **109**, 18 701–18 706, doi: 10.1073/pnas.1210239109.

Meehl, G. A., and A. X. Hu, 2006: Megadroughts in the Indian monsoon region and southwest North America and a mechanism for associated multidecadal Pacific sea surface temperature anomalies. *J Climate*, **19**, 1605–1623, doi: 10.1175/JCLI3675.1.

Power, S., T. Casey, C. Folland, A. Colman, and V. Mehta, 1999: Inter-decadal modulation of the impact of ENSO on Australia. *Climate Dyn*., **15**, 319–324, doi: 10.1007/s003820050284.

Rayner, N. A., D. E. Parker, E. B. Horton, C. K. Folland, L. V. Alexander, D. P. Rowell, E. C. Kent, and A. Kaplan, 2003: Global analyses of sea surface temperature, sea ice, and night marine air temperature since the late nineteenth century. *J. Geophys. Res*., **108**, 4407, doi: 10.1029/2002JD002670.

Saji, N. H., and T. Yamagata, 2003: Possible impacts of Indian Ocean Dipole mode events on global climate. *Climate Research*, **25**, 151–169, doi: 10.3354/cr025151.

Saji, N. H., B. N. Goswami, P. N. Vinayachandran, and T. Yamagata, 1999: A dipole mode in the tropical Indian Ocean. *Nature*, **401**, 360–363.

Saji, N. H., S.-P. Xie, and T. Yamagata, 2006: Tropical Indian Ocean variability in the IPCC twentieth-century climate simulations. *J. Climate*, **19**, 4397–4417, doi: 10.1175/JCLI3847.1.

Tozuka, T., J. J. Luo, S. Masson, and T. Yamagata, 2007: Decadal modulations of the Indian Ocean dipole in the SINTEX-F1 coupled GCM. *J. Climate*, **20**, 2881–2894, doi: 10.1175/JCLI4168.1.

Webster, P. J., A. M. Moore, J. P. Loschnigg, and R. R. Leben, 1999: Coupled ocean–atmosphere dynamics in the Indian Ocean during 1997–98. *Nature*, **401**, 356–360, doi: 10.1038/43848.

Wu, L., Z. Liu, R. Gallimore, R. Jacob, D. Lee, and Y. Zhong, 2003: Pacific decadal variability: The tropical Pacific mode and the North Pacific mode. *J. Climate*, **16**, 1101–1120, doi: 10.1175/1520-0442(2003)16<1101:PDVTTP>2.0.CO;2.

Xie, S.–P., C. Deser, G. A. Vecchi, J. Ma, H. Y. Teng, and A. T. Wittenberg, 2010: Global warming pattern formation: Sea surface temperature and rainfall. *J. Climate*, **23**, 966–986, doi: 10.1175/2009JCLI3329.1.

Yamagata, T., S. K. Behera, J.-J. Luo, S. Masson, M. R. Jury, and S. A. Rao, 2004: Coupled ocean–atmosphere variability in the tropical Indian Ocean. *Earth's Climate: The Ocean–Atmosphere Interaction*, vol. 147, *Geophysical Monograph Series*, C. Wang, S. P. Xie, and J. A. Carton, Eds., American Geophysical Union, 189–212, doi: 10.1029/147GM12.

Yang, Y., L. X. Wu, and C. F. Fang, 2012: Will global warming suppress North Atlantic Tripole decadal variability? *J. Climate*, **25**, 2040–2055, doi: 10.1175/JCLI-D-11-00164.1.

Yang, Y., S.-P. Xie, L. X. Wu, Y. Kosaka, N.-C. Lau, and G. A. Vecchi, 2015: Seasonality and predictability of the Indian Ocean dipole mode: ENSO forcing and internal variability. *J. Climate*, **28**, 8021–8036, doi: 10.1175/JCLI-D-15-0078.1.

Yang, Y., S.-P. Xie, L. X. Wu, Y. Kosaka, and J. P. Li, 2017: ENSO forced and local variability of North Tropical Atlantic SST: Model simulations and biases. *Climate Dyn*., doi: 10.1007/s00382-017-3679-9.

Yu, J.-Y., and K. M. Lau, 2004: Contrasting Indian Ocean SST variability with and without ENSO influence: A coupled atmosphere–ocean GCM study. *Meteor. Atmos. Phys*., **90**, 179–191, doi: 10.1007/s00703-004-0094-7.

Yu, J.-Y., C. R. Mechoso, J. C. McWilliams, and A. Arakawa, 2002: Impacts of the Indian Ocean on the ENSO cycle. *Geophys. Res. Lett*., **29**(8), 46-1–46-4, doi: 10.1029/2001GL014098.

Zhang, Y., J. M. Wallace, and D. S. Battisti, 1997: ENSO-like interdecadal variability: 1900–93. *J. Climate*, **10**, 1004–1020, doi: 10.1175/1520-0442(1997)010<1004:ELIV>2.0.CO;2.

Zheng, X. T., S.-P. Xie, G. A. Vecchi, Q. Y. Liu, and J. Hafner, 2010: Indian Ocean dipole response to global warming: Analysis of ocean–atmospheric feedbacks in a coupled model. *J. Climate*, **23**, 1240–1253, doi: 10.1175/2009JCLI3326.1.